A role for neuronal cAMP responsive-element binding (CREB)-1 in brain responses to calorie restriction

Salvatore Fusco[a], Cristian Ripoli[b], Maria Vittoria Podda[b], Sofia Chiatamone Ranieri[a,1], Lucia Leone[b], Gabriele Toietta[c], Michael W. McBurney[d], Günther Schütz[e], Antonella Riccio[f], Claudio Grassi[b], Tommaso Galeotti[a], and Giovambattista Pani[a,2]

[a]Laboratory of Cell Signaling, Institute of General Pathology, and [b]Institute of Human Physiology, Universita' Cattolica School of Medicine, 00168 Rome, Italy; [c]Department of Laboratory Medicine, Ospedale Pediatrico Bambino Gesù-Istituto di Ricovero e Cura a Carattere Scientifico, 00165 Rome, Italy; [d]Department of Medicine, Center for Cancer Therapeutics, Ottawa Hospital Research Institute, University of Ottawa, Ottawa, ON, Canada K1H 8L6; [e]Division of Molecular Biology of the Cell I, German Cancer Research Center (DKFZ), 69120 Heidelberg, Germany; and [f]Department of Neuroscience, Physiology, and Pharmacology, Medical Research Council Laboratory for Molecular and Cell Biology, University College London, London WC1E 6BT, United Kingdom

Edited* by Marc Montminy, The Salk Institute for Biological Studies, La Jolla, CA, and approved December 2, 2011 (received for review June 9, 2011)

Calorie restriction delays brain senescence and prevents neurodegeneration, but critical regulators of these beneficial responses other than the NAD$^+$-dependent histone deacetylase Sirtuin-1 (Sirt-1) are unknown. We report that effects of calorie restriction on neuronal plasticity, memory and social behavior are abolished in mice lacking cAMP responsive-element binding (CREB)-1 in the forebrain. Moreover, CREB deficiency drastically reduces the expression of Sirt-1 and the induction of genes relevant to neuronal metabolism and survival in the cortex and hippocampus of dietary-restricted animals. Biochemical studies reveal a complex interplay between CREB and Sirt-1: CREB directly regulates the transcription of the sirtuin in neuronal cells by binding to Sirt-1 chromatin; Sirt-1, in turn, is recruited by CREB to DNA and promotes CREB-dependent expression of target gene peroxisome proliferator-activated receptor-γ coactivator-1α and neuronal NO Synthase. Accordingly, expression of these CREB targets is markedly reduced in the brain of Sirt KO mice that are, like CREB-deficient mice, poorly responsive to calorie restriction. Thus, the above circuitry, modulated by nutrient availability, links energy metabolism with neurotrophin signaling, participates in brain adaptation to nutrient restriction, and is potentially relevant to accelerated brain aging by overnutrition and diabetes.

Progressive decline of cognitive functions and an increased risk of developing neurodegenerative disorders, such as Alzheimer's and Parkinson diseases, are severe and debilitating consequences on brain senescence. A moderate reduction of food intake (calorie restriction, CR) delays aging and improves resistance to disease in a fashion that is evolutionarily conserved from yeast to primates and humans (1), and these beneficial effects include in mammals the prevention of age-associated cognitive impairment and neurodegeneration (2). Conversely, obesity and type 2 diabetes increase the risk of developing Alzheimer's disease (AD) (3), and reduced insulin signaling in the brain may contribute to neurodegeneration (4). Elucidation of the molecular mechanisms whereby nutritional/metabolic cues impinge on neuronal survival and health may be an avenue to new pharmacological strategies that exploit nutrient-sensitive protective circuitries to prevent the catastrophic impact of aging and dysmetabolism on the brain.

Most of the current molecular knowledge on the beneficial effects of CR involves Sirtuins, the mammalian homologs of the yeast Silent Information Regulator (Sir2.1) NAD$^+$-dependent histone deacetylase (5, 6). This class of enzymes plays an evolutionarily conserved role in promoting genomic stability, cell survival, and stress resistance in response to limited nutrient availability. Such action results in extended longevity in lower organisms, and prevents in mammals a variety of age-associated pathologic changes from cardiovascular disease and diabetes, to cancer, to neurologic disorders. In particular, neuronal Sirt-1 has been shown to regulate endocrine and behavioral responses to CR (7) and to prevent AD amyloid neuropathology in dietary-restricted mice (8, 9). To date, however, the nutrient-sensitive signaling cascades upstream of sirtuins, as well as their downstream molecular effectors, have been incompletely characterized, especially in the brain.

Another class of neuroprotective factors, neurotrophins, promotes neuronal cell health by triggering genetic programs that are largely dependent on the cAMP responsive-element binding (CREB) factor (10, 11); accordingly, neurotrophin and CREB activities are critically reduced in the context of aging and of age-associated brain diseases (12–14). Of note, CREB also serves as a metabolic sensor in several tissues, including the brain (15), and a functional interplay between CREB and Sirt-1 in neurons through miR134 has been recently reported (16). It is therefore conceivable that CREB integrates neurotrophic and metabolic signals in the orchestration of complex neuroprotective responses that oppose brain aging.

This attractive hypothesis prompted us to investigate whether: (*i*) neuronal CREB has a role in brain response to CR and, by extension, in the metabolic regulation of brain function and health in mice; and (*ii*) this unique CREB function involves molecular interactions with Sirt-1.

Results

Effects of CR on Long-Term Potentiation, Memory, and Behavior Are Impaired in Mice Lacking Neuronal CREB. Mice subject to moderate CR display behavioral (increase in physical and exploratory activity) and cognitive (improved object memory and spatial learning) changes largely related to increased wakefulness and food-seeking (17, 7). To explore the potential role of CREB in brain response to dietary restriction, we took advantage of a "floxed" conditional mutant mouse strain (*CREB1*$^{loxP/loxP}$) in which postnatal inactivation of the gene in the forebrain is driven by a Cre recombinase transgene under the transcriptional control of the calcium/calmodulin-dependent protein kinase II-α gene (*Camk2a*) promoter (18). Brain immunostaining of 6-mo-old CREB$^{loxP/loxP}$-Camk*Cre*$^+$ (henceforth indicated as BCKO, Brain CREB KO) male mice confirmed a dramatic reduction of CREB1 signal in cortex and hippocampus compared with control littermates (Fig. 1*Aa*). These mice appear phenotypically normal, although slightly smaller than their recombinase-negative littermates (CREB$^{loxP/loxP}$ Camk*Cre* negative, henceforth "control" mice) (Fig. 1*Ab*). BCKO mice and their CREB-proficient controls were left with free

Author contributions: S.F. and G.P. designed research; S.F., C.R., M.V.P., S.C.R., L.L., and G.T. performed research; G.T., M.W.M., and G.S. contributed new reagents/analytic tools; S.F., C.R., M.V.P., S.C.R., L.L., A.R., C.G., T.G., and G.P. analyzed data; G.P. wrote the paper; and C.G. supervised long-term potentiation studies.

The authors declare no conflict of interest.

*This Direct Submission article had a prearranged editor.

[1]Present address: Clinical Chemistry, Laboratory and Endocrinology Unit, Departement of Laboratory Medicine, Azienda Ospedaliera ASMN, Istituto di Ricovero e Cura a Carattere Scientifico, Reggio Emilia, Italy.

[2]To whom correspondence should be addressed. E-mail: gpani@rm.unicatt.it.

This article contains supporting information online at www.pnas.org/lookup/suppl/doi:10.1073/pnas.1109237109/-/DCSupplemental.

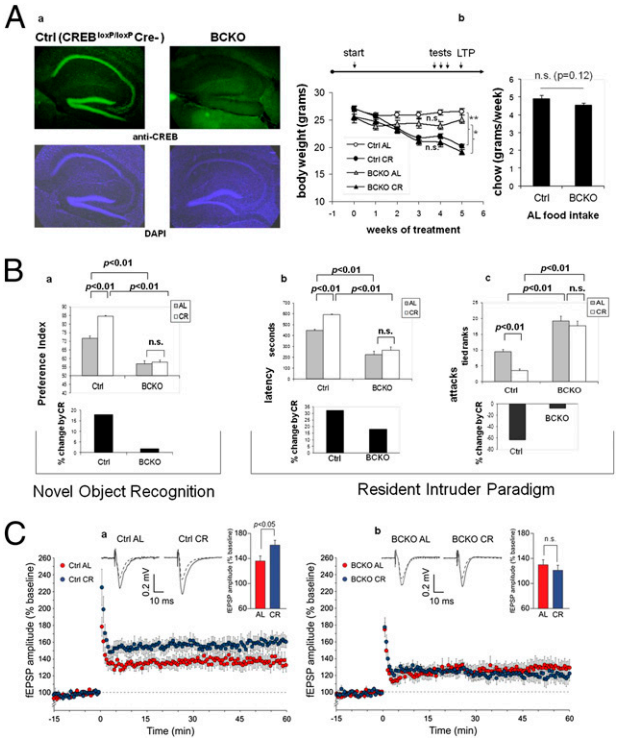

Fig. 1. Impaired brain response to calorie restriction in mice lacking neuronal CREB. (*Aa*) Immunofluorescence analysis reveals a near complete deletion of CREB1 in the cortex and hippocampus of 6-mo-old BCKO mice. Nuclear staining with DAPI confirms normal cellularity in the same areas. (*b*) Weight loss under calorie restriction (*Left*) and food consumption ad libitum (*Right*) in control (Ctrl) and BCKO mice (n = 5–6 per group, one of two independent experiments); (*Left*) $^{**}P < 0.01$; $^{*}P < 0.05$; n.s. nonsignificant by two-way ANOVA (4 wk time-point); (*Right*) P by two-tailed t test. (*B*) Cognitive and behavioral effects of CR. (*a*) (*Upper*) Preference toward the novel object in a novel object recognition paradigm. Values (seconds) are mean ± SEM. (*Lower*) Percent change by CR. (*b* and *c*) (*Upper*) Latency of the first attack (*Left*, values in seconds, mean ± SEM) and number of attacks in 10 min (*Right*, rank in an ordinal scale ± SEM) were scored in a resident-intruder paradigm. (*Lower*) Percentage changes of the corresponding parameter by calorie restriction in control and BCKO mice datasets (n = 6 animals per group) were analyzed by two-way ANOVA; P values are indicated. Experiments were performed twice with similar results. (*C*) Time course of Schaffer collateral-CA1 LTP induced by tetanic stimulation in control (*a*) and BCKO (*b*) mice. Values are percentages of baseline fEPSP amplitude (100%). (*Insets*) Representative fEPSPs at baseline (dashed line) and during the last 10 min of LTP recording (solid line). Traces are averages of 10 consecutive responses at the time points selected. Bar graphs compare average LTP magnitudes observed during the last 10 min of recording (percentage of baseline fEPSP amplitude). (Student t test, $^{*}P < 0.05$).

access to food (*Ad libitum* regimen, AL) or subject to a CR regimen (70% of the AL food intake of the corresponding genotype) for a period of 5 wk; food consumption, and effect of food restriction on body weight, both monitored weekly, were comparable in the two strains (Fig. 1*Ab*), indicating that neither feeding behavior nor gross energy metabolism were affected in mutant mice.

We first asked whether CREB deletion affected the beneficial effect of CR on the cognitive performance of our mice. To this end, a standard novel object recognition paradigm (19) was used to assess object memory 24 h after a training section. We found that preference for the novel object (expressed as preference index) was significantly more pronounced in control than in BCKO mice (Fig. 1*Ba*), consistent with a reported role for CREB in memory consolidation (20). Importantly, memory performance was clearly improved by CR in control mice ($P < 0.01$ by bifactorial ANOVA) but not in the BCKO strain (Fig. 1*Ba*), suggesting a major role for CREB in the effect of nutrient restriction on this cognitive task.

CR reduces male aggressiveness in mice, most likely by acting on the brain serotoninergic system (21). Prompted by the observation that BCKO male mice appeared more aggressive than their control littermates, we decided to investigate this aspect in detail in the context of a resident-intruder paradigm (22). BCKO mice fed AL attacked the intruder with shorter latency (Fig. 1*Bb*) and higher frequency (Fig. 1*Bc*) compared with controls, confirming a more aggressive behavior of these animals. This behavior phenocopies that of mice lacking neuronal nitric oxide synthase (nNOS) (22), an enzyme transcriptionally regulated by CREB (23). Aggressiveness was markedly diminished in CR control mice compared with littermates fed AL ($P < 0.01$, two-way ANOVA); conversely, BCKO mice showed only a marginal decrease of aggressive behavior in response to food restriction (Fig. 1*B*, *b* and *c*). Thus, neuronal CREB appears to be necessary for at least some of the cognitive and behavioral changes induced by CR in mice. Importantly, additional controls ruled out the possibility that the small difference in food intake between control and BCKO mice or the expression of the Cre recombinase per se in the latter strain may contribute to the above CREB-related phenotypic changes (Fig. S1).

Long-term potentiation (LTP) in the hippocampus underlies higher-order brain functions, including object and spatial memory. This indicator of neuronal plasticity declines in rodents with age, in a fashion that is attenuated by calorie restriction (24). To extend our analysis of CR effects on the brain of CREB-deficient mice, we tested LTP at CA3-CA1 synapses in hippocampal brain slices obtained from animals euthanized after 5 wk of either CR or AL feeding regimen. As previously shown (25), LTP was not affected by CREB status in the two AL-fed groups. Strikingly, however, LTP increased in control mice under CR [AL 136.6 ± 8.0% (n = 10 slices) vs. CR 161.3 ± 8.2% (n = 9 slices); $P < 0.05$] but not in the BCKO strain [AL 130.3 ± 8.6% (n = 9 slices) vs. CR 121.0 ± 8.5% (n = 10 slices), n.s.] (Fig. 1*C*), indicating that beneficial effect of CR on LTP is also abrogated by brain-specific CREB deletion. The increased LTP induced by CR in control mice was independent on changes in basal synaptic transmission, because input/output curves obtained plotting field excitatory postsynaptic potential (fEPSP) amplitudes vs. stimulus intensity in hippocampal brain slices of CR and AL animals were superimposable.

Brain CREB Is Activated by CR and Increases the Expression of Sirt-1. Because CREB appeared to participate in brain response to CR, we assessed whether diet affected the total amount/phosphorylation of CREB protein, and the expression level of a number of mRNAs known to be regulated by CREB (23). CREB1 protein expression in control mice was not changed by the dietary regimen; instead, an increase in CREB phosphorylation on Serine 133 in the hippocampi of the CR group was revealed by phospho-specific immunoblotting (Fig. 2*A*), suggesting that CR activates CREB in this brain area. Accordingly, mRNAs of "canonical" CREB targets peroxisome proliferator-activated receptor-γ coactivator-1α (*PGC-1α*), *nNOS*, and phosphoenolpyruvate carboxykinase (*PEPCK*) were induced by CR in the cortex and hippocampus of CREB-proficient mice (Fig. 2*B*). Of note, both PGC-1α and NO, the product of NOS enzymes, are known to promote mitochondrial biogenesis and to participate in organismal response to CR (26). The three mRNAs were overall down-regulated in BCKO mice fed AL compared with controls, and their induction by CR, observed in control mice, was nearly abolished (Fig. 2*B*). Interestingly, the expression of other putative CREB targets like *bcl-2*, *NGF*, and *c-fos* were unaffected by CR and CREB deletion (Fig. S2). Thus, collectively, these findings demonstrate that nutrient availability selectively regulates CREB-dependent gene expression in the forebrain.

We next asked how CR may affect CREB activity. Because Sirt-1 is a metabolic sensor involved in several biological consequences of nutrient deprivation (27, 6), and animals lacking Sirt-1 in the brain show defective behavioral and hormonal responses to CR (7), we investigated the sirtuin as a potential CREB interactor.

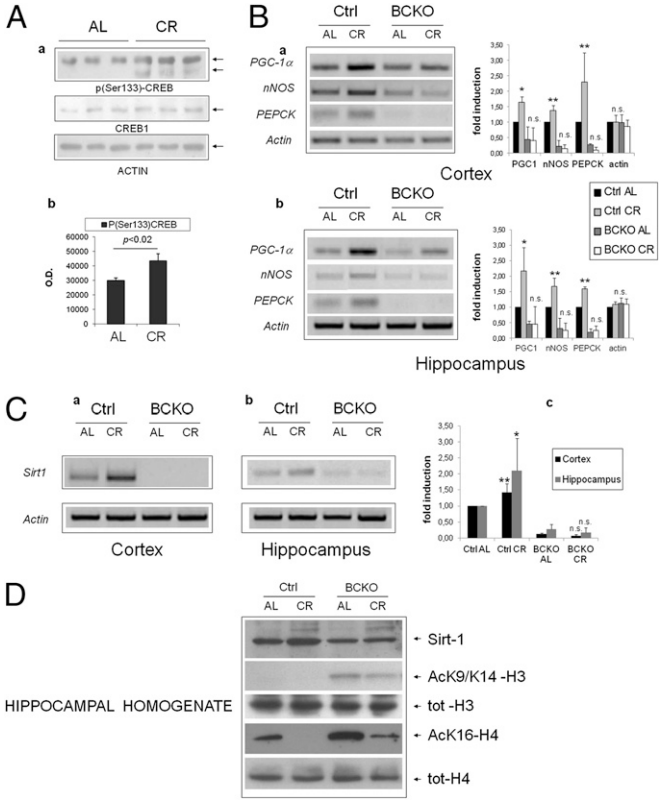

Fig. 2. Brain CREB is activated by calorie restriction and increases the expression of Sirt-1. (*Aa*) Western blot analysis of hippocampal homogenates from individual mice revealing increased phosphorylation of CREB on Ser-133 by calorie restriction. (*b*) Band densitometry normalized to actin; statistics by two-tailed *t* test. (*B*) RT-PCR analysis of three canonical CREB target mRNAs in the cortex (*a*) and hippocampus (*b*) of control and BCKO mice after 4 wk of AL or CR feeding. Actin was used as loading control. Histograms report fold-induction values compared with Ctrl AL (mean ± SD of three to five mice). $*P < 0.05$; $**P < 0.01$; n.s., nonsignificant by two-way ANOVA (CR vs. AL). (*C*) RT-PCR analysis of Sirt-1 mRNA expression and up-regulation by CR in the cortex (*a*) and hippocampus (*b*) of control and BCKO mice. Histogram in *c* displays fold-induction values relative to Ctrl AL (mean ± SD of three to five mice). Statistics as in *B*. (*D*) Western blot analysis of hippocampal homogenates showing impaired up-regulation of Sirt-1 by CR and increased acetylation of histones H3 and H4 at Sirt-1-sensitive sites in BCKO mice. Anti-total H3 and H4 histones confirms equal protein input throughout the lanes. Each lane is the pool of hippocampi from two different mice.

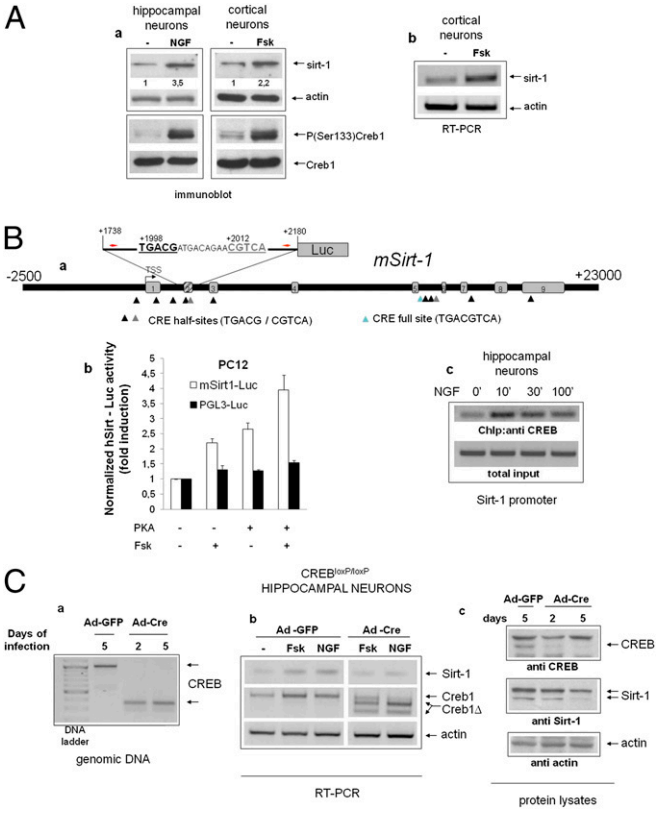

Fig. 3. Transcriptional regulation of Sirt-1 by CREB in neuronal cells. (*Aa*) Immunoblot analysis of whole-cell lysates from primary neurons (hippocampal or cortical) exposed to CREB-activating stimuli. NGF, 50 ng/mL; Fsk, 10 μM. Relevant bands are indicated by arrows. Relative densitometric values for the Sirt-1 band are indicated. CREB phosphorylation and Sirt-1 expression were assayed at different times (30 min and 16 h, respectively). (*b*) RT PCR analysis of Sirt-1 mRNA in cortical neurons treated with Fsk for 6 h. Actin was amplified as an internal loading control. Panels representative of several independent experiments. (*Ba*) Scheme displaying several putative CRE elements within the mouse *Sirt-1* gene (MGSCv37 C57BL/6J, locus NC_000076). The segment inserted in the Sirt-1-Luc reporter gene, and primers used in ChIP studies (red arrows) are indicated. Two CRE half-sites internal to the segment are also highlighted; numbers are positions relative to the annotated TSS. Exons refer to transcript variant 1. The exon 2 box is shaded because this exon is absent in transcript variants 2 and 3. (*b*) Luciferase reporter assay confirming responsiveness of the 1738–2180 genomic fragment to Fsk and PKA in PC12 cells. Bars are fold-induction ± SD of triplicate samples; picture representative of two independent experiments. (*c*) ChIP assay showing NGF-induced binding of CREB to the 1824–2090 Sirt-1 region in hippocampal neurons. Minutes of stimulation are indicated. Sirt-1 promoter was amplified from the total chromatin input as quantitative control (*Lower*). (*Ca*) Deletion of CREB exon 10 in cultured $CREB^{loxP/loxP}$ hippocampal neurons 2 or 5 d after adenoviral delivery of Cre recombinase (Ad-Cre). Genomic DNA was amplified with two primers external to the recombination sites. Bands corresponding to undeleted (*Upper*) and deleted (*Lower*) alleles are indicated by arrows. (*b*) RT-PCR analysis revealing defective induction of Sirt-1 mRNA by NGF and Fsk (6 h) in CREB-deleted hippocampal neurons. Actin was amplified as loading control. Bands corresponding to deleted (ΔCREB) and residual undeleted CREB mRNA are indicated by arrows. Picture is representative of several independent experiments. (*c*) Western blot analysis of whole cell lysates from mock (Ad-GFP) and Cre-infected cells indicating reduced expression of Sirt-1 in the latter cell population. Actin band confirms equal protein loading.

Sirt-1 mRNA was drastically reduced both in the cortex and hippocampus of BCKO mice, irrespective of the dietary regimen. Moreover, the moderate induction by CR that we observed in control brains was completely lost in the corresponding CREB-deficient tissues (Fig. 2*C*). Finally, acetylation of Histones H3 (AcK9) and H4 (AcK16), an inverse correlate of Sirt-1 activity (28), was abnormally high in BCKO hippocampal homogenates (Fig. 2*D*), confirming an overall reduction of Sirt-1 activity in this area of the brain.

Transcriptional Regulation of Sirt-1 by CREB in Neurons. These observations suggested that Sirt-1 may represent a direct transcriptional target of CREB. Accordingly, CREB activators NGF and Forskolin (Fsk) (29) raised the level of immunoreactive Sirt-1 and of the corresponding mRNA in cultured primary cortical and hippocampal neurons (Fig. 3*A*). Bioinformatic analysis of the mouse *Sirt-1* locus (NC_000076) revealed the presence of several putative cAMP Responsive Elements (CRE) both upstream and downstream of the transcription start site (TSS) (30), and an ∼300-bp segment encompassing two of those elements (TGACG at +1,998 and CGTCA at +2,012 from the annotated TSS) drove transcriptional response to Fsk and PKA in a standard luciferase reporter assay performed in PC12 pheochromocytoma cells (Fig. 3*B*, *a* and *b*). Moreover, ChIP from hippocampal neurons revealed that CREB binds the same genomic region in a fashion inducible

NEUROSCIENCE

by NGF (Fig. 3*Bc*). Finally, in primary neurons isolated from CREB$^{loxP/loxP}$ mice, deletion of CREB by adenoviral delivery of the *Cre* recombinase (Fig. 3*C*, *a* and *b*) led to a reduction of Sirt-1 immunoreactivity (Fig. 3*Cc*), and inhibited Sirt-1 mRNA induction by NGF and Fsk (Fig. 3*Cb*). Thus, we conclude that CREB directly regulates Sirt-1 mRNA and protein expression in neurons.

Sirt-1 Binds CREB and Promotes CREB-Dependent Gene Expression. Known transcriptional regulators of Sirt-1, such as p53 and Foxo3a (31), also interact with, and are either positively or negatively modulated by the deacetylase (32, 33); similarly, a myc-tagged form of human CREB1 and Sirt-1 could be easily coimmunoprecipated in naive PC12 cells (Fig. 4*A*), indicating physical association between the two proteins; the association was rapidly induced by the PKA agonist Fsk, in parallel with phosphorylation of CREB on Serine 133. Short-time (30 min) stimulation with Fsk did not affect the total amount of cellular Sirt-1, but rather increased the stoichiometry of the binding to CREB, suggesting either an increased affinity between the two proteins, or the enhanced interaction with intermediate molecular partners co-recruited at target gene promoters. In keeping with the latter possibility, a mutant CREB that retains the phosphorylation site but is unable to bind DNA because of the deletion of the C-terminal transactivation domain (ΔLZ CREB), displayed marginal physical interaction with Sirt-1, nor was the binding induced by Fsk (Fig. 4*A*).

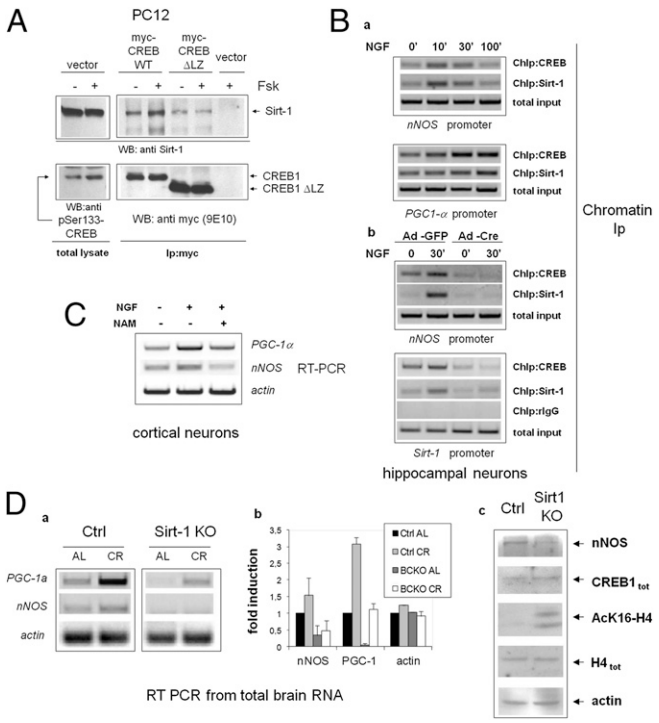

Fig. 4. Sirt-1 promotes CREB-dependent gene expression. (*A*) Forskolin-inducible physical association of CREB with Sirt-1 in PC12 cells. mycCREB or mycCREB-ΔLZ were transfected in PC12 cells and immunoprecipitated from protein lysates untreated or stimulated with Fsk for 30 min; the presence of Sirt-1 in immunocomplexes was verified by immunoblotting (*Upper*); anti-Ser133 CREB and anti-myc immunoblotting were used to confirm CREB phosphorylation by Fsk and assess the expression level of transfected CREB isoforms, respectively (*Lower*). (*Ba*) ChIP assays showing parallel interaction of CREB and Sirt-1 with the CRE-containing promoter regions of *nNOS* and *PGC-1α* in hippocampal neurons treated with NGF. Promoter amplification from total chromatin input is also reported as control. (*b*) CREB mediates Sirt-1 interaction with CRE-containing promoter regions. NGF-inducible binding of Sirt-1 to *nNOS* (*Upper*) and *Sirt-1* promoter (*Lower*) are drastically reduced in hippocampal neurons lacking CREB. Binding of CREB to the same promoter regions confirms severe reduction of CREB binding in Cre-infected cells. rIgG (rabbit IgG) is a negative control for ChIP. Total chromatin input was equal throughout the lanes. (*C*) RT-PCR analysis showing reduced induction of *nNOS* and *PGC-1α* mRNA by NGF in cortical neurons treated with the Sirt-1 inhibitor Nicotinamide (NAM). (*D*) (*a* and *b*) Representative RT-PCR analysis of *PGC-1α* and *nNOS* mRNA expression in whole brains from WT and Sirt-1-deficient mice under both AL and CR (6 mo) feeding. Each lane represents a pool of two mice. Actin was used as loading control. (*c*) Western blot analysis of whole brain protein homogenates from WT and Sirt-1 KO mice (fed AL) indicating reduced expression of nNOS but normal levels of immunoreactive CREB and total histone H4. Anti-AcH4K16 and antiactin immunostaining confirm, respectively, reduced deacetylase activity in the SirtKO sample and equal protein loading in the two lanes.

To confirm that SIRT1 and CREB colocalize on CREB-responsive chromatin regions in cortical neurons, cross-linked chromatin was immunoprecipitated with an anti-Sirt-1 antiserum and Sirt-1 binding to the regions of *nNOS* and *PGC-1α* promoters surrounding the CRE elements determined by semiquantitative PCR. Sirt-1 was found to interact with both genes, in a fashion inducible by NGF and with a binding kinetic similar to that of CREB (Fig. 4*Ba*). Sirt-1 also bound the same *Sirt-1* chromatin region surrounding the +1,998/+2,012 half-CRE sites that coprecipitates with CREB, suggesting that Sirt-1 may self-regulate its CRE-dependent transactivation (Fig. 4*Bb*). Of note, Sirt-1 interaction with *nNOS* and *Sirt-1* chromatin was indeed mediated by CREB, as revealed by its drastic reduction in CREB $^{loxP/loxP}$ neurons following the recombinase-mediated deletion of the factor (Fig. 4*Bb*) and by the failure of forced Sirt-1 overexpression to restore Sirt-1 chromatin binding in CREB-deficient cells (Fig. S3).

To determine whether Sirt-1 modulates CREB transcriptional activity, cortical neurons were stimulated with NGF in the presence of sirtuin inhibitor Nicotinamide (34); induction of *nNOS* and *PGC-1α* mRNA by NGF was blunted upon inhibition of Sirt-1 deacetylase activity (Fig. 4*C*). A similar result was obtained in naive PC12 cells by siRNA-mediated knock-down of Sirt-1 (Fig. S4*A*). In addition, Sirt-1–deficient PC12 displayed impaired differentiation by NGF (as assessed by quantification of neurite outgrowth), a response largely dependent on CREB and nNOS in this cell model (35, 36) (Fig. S4*B*). In a complementary set of experiments, lentivirus-mediated overexpression of Sirt-1 increased the expression of *nNOS* and *PGC-1α* mRNA in hippocampal neurons treated with NGF. However, Sirt-1 did not fully restore the expression of these genes in CREB-deficient cells, nor NGF protection from hydrogen peroxide-dependent cell death, which is largely lost in these cells (Fig. S5), was recovered upon transduction of the Sirt-1 cDNA. Collectively, the above data suggest that Sirt-1 and CREB are, at least to some extent, reciprocally dependent, and act in concert in the context of neurotrophin signaling.

Unlike previously reported findings (16), manipulations aimed at modulating Sirt-1 expression and activity in the above contexts did not affect the level of immunoreactive CREB1 (Fig. S4*Aa*).

Defective Expression of CREB Target Genes in the Brain of CR Sirt-1 KO Mice. Finally, to verify whether Sirt-1 actually regulates CREB-dependent transcription in vivo and this is relevant for response to CR, we analyzed the expression of CREB targets *nNOS* and *PGC-1α* mRNAs in whole brains of Sirt-1 KO mice fed AL or CR for 25–28 wk (37). This analysis revealed that both genes are markedly hypoexpressed in Sirt-deficient mice compared with littermate controls under both dietary regimens (Fig. 4*D*), and their induction by CR, that was more pronounced for PGC-1α, was also attenuated (Fig. 4*D*, *a* and *b*). The amount of immunoreactive CREB was comparable in brain homogenates of the two strains (Fig. 4*Dc*), nor CREB acetylation on lysine residues was affected by either Sirt-1 deletion or CR (Fig. S6), indicating that, at least in these experimental settings, Sirt-1 regulates CREB transcriptional activity independent of the acetylation and expression level of the factor.

Taken together, the above findings strongly suggest that Sirt-1 modulates the expression of CREB-dependent genes in mouse brain, and by extension, identify in the decrease of CREB-

dependent transcription a molecular signature for a defective brain response to CR, shared by CREB and Sirt-1 mutant mice (7).

Discussion

The CREB transcription factor has been widely investigated as a metabolic sensor and regulator of glucose homeostasis in liver and fat tissue (15), and as a master switch of calcium and neurotrophin-triggered transcriptional programs regulating neuronal differentiation, survival, and plasticity in the brain and peripheral nervous system (10, 11, 18). Evidence also exist for CREB roles in the control of appetite and food intake in the hypothalamus (38), but whether neuronal plasticity and high-order cognitive functions may be influenced by nutrient cues and energy metabolism through CREB, an issue relevant to major diseases like AD and type 2 diabetes (3, 4), remains to be established. Our demonstration of impaired electrophysiological, cognitive, and emotional response to CR in brain CREB KO mice, clearly suggests that this may indeed be the case. Interestingly, these differences emerge in the context of an overall comparable feeding behavior and metabolic response to CR between control and BCKO mice (Fig. 1*Ab*), indicating that potential effects of hypothalamic CREB signaling on energy balance and appetite regulation unlikely account for the observed phenotypes (38).

Data reported in Fig. 2, showing CREB phosphorylation and transcriptional activation by CR, indicate that CREB is metabolically regulated in the cortex and hippocampus, although the mechanism of such regulation needs to be further investigated. Because plasma from CR rodents has been previously shown to induce Sirt-1 expression in several organs/tissues, a humoral/hormonal mechanism for CREB activation could be envisaged (39); as an alternative, NO (40) or oxygen species (41) may mediate, cell-autonomously, this effect. Further research in this direction is warranted.

Our data identify in the complex interplay with the nutrient-sensitive histone deacetylase Sirt-1 a molecular connection between CREB and neuronal response to CR. Previous work from others has compellingly involved neuronal Sirt-1 in hormonal and metabolic adaptation to dietary restriction in mice (7). Results presented here clearly suggest that the two molecules are part of the same CR-sensitive signaling cascade. However, other genes potentially relevant to mitochondrial biogenesis and neuronal response to calorie restriction, namely *nNOS* and *PGC-1α* (40), and some *PGC-1α* targets—including *CPT1*, *CoxIV*, and *UCP-2*—are also critically down-regulated, together with Sirt-1, in the cortex and hippocampus of BCKO mice (Fig. 2*B* and Fig. S2*b*). This finding, and evidence from Fig. S3 that overexpression of Sirt-1 does not rescue NGF signaling in CREB-deficient hippocampal neurons in vitro, suggests that up-regulation of Sirt-1 is not the only mechanism whereby CREB participates in neuronal response to nutrients. Instead, cooperation with CREB is likely critical for the action of neuronal Sirt-1 in CR. This view is supported by the unexpected finding that CREB-dependent genes involved in neuronal plasticity, survival, and stress resistance (42, 43), and induced by calorie restriction (Fig. 2), are markedly down-regulated in Sirt-1–deficient cultured neurons (PC12) and in the brain of Sirt-1 KO mice. Because the latter strain is, like BCKO mice, impaired in brain response to reduced food intake (7), the above evidence further support the notion that CREB-dependent transcription has a pivotal role in the neuronal effects of calorie restriction, and identify in the CREB–Sirt-1 axis a major component of the nutrient sensitive molecular network that connects caloric intake and energy metabolism to brain health.

Biochemical details of how Sirt-1 affects CREB activity remains to be clarified. Unlike other transcription factors, CREB does not appear to be deacetylated by Sirt-1 (Fig. S6); moreover, we could not detect consistent effects of Sirt-1 on the expression of CREB (Fig. 4*Dc*, and Figs. S4*Aa* and S6), unlike that described by Gao et al. (16). Those authors, however, made their important observations on Sirt-1 $^{\Delta ex4}$ mice that, unlike Sirt-1KO mice used in our experiments, do express an inactive form of Sirt-1 potentially acting in a dominant negative fashion against other molecules (deacetylases?) capable of regulating CREB expression.

On the other hand, Sirt-1 dependent modulation of nutrient sensitive cofactors of CREB, like TORC/Crtc (38), has been described in the liver and may occur in neuronal cells. Alternatively, Sirt-1 may be recruited by CREB on target promoters and act either on histones (Fig. 2*D*) or, *in trans*, on other (maybe competing) transcription factors.

In conclusion, CREB1, an effector of neurotrophins involved in several age-associated neurodegenerative diseases, mediates at least some brain responses to dietary restriction. This action involves the up-regulation of Sirt-1 that in turn bolsters the CREB-dependent expression of genes involved in neuronal metabolism, survival and plasticity (Fig. S7). Although molecular details on how Sirt-1 regulates gene transcription by CREB need to be further investigated, the CREB-Sirt-1 axis outlines a unique molecular network at the crossroad of energy metabolism, metabolic diseases, and brain aging.

Materials and Methods

Mice. BCKO (*CREB1*$^{loxP/loxP}$- *Camk2aCRE)* mice, Sirt-1 KO mice, and the relative control strains have been previously described elsewhere (18, 37).

Calorie Restriction. For CR studies, the amount of food consumed by AL mice was determined weekly, and CR mice were fed daily 80% of that value for the first week and 60% for the following 4 wk. Absolute food consumption AL was slightly (about 10%) higher in control than in BCKO mice, but the amount of chow per gram body weight comparable, because of the smaller size of the latter strain. CR in BCKO mice was calculated either on the AL feeding of mice of the same genotype, or on the AL consumption of control mice, with similar results. Body weight was monitored weekly.

Behavioral Tests. All behavioral tests were conducted on male, 6-mo-old mice, during the dark cycle (the animals' active phase). Resident-intruder and novel object recognition paradigms were performed according to refs. 11 and 13, respectively, with minimal changes.

Long-Term Potentiation. Coronal hippocampal slices (400-μm thick) were obtained from adult male C57BL/6 mice. fEPSP evoked by Schaffer collateral stimulation were recorded from the CA1 subfield of the hippocampus. The stimulation intensity that produced one-third of the maximal response was used for the test pulses and LTP induction protocol consisting of four trains of 50 stimuli at 100 Hz repeated every 20 s (referred to as tetanus). The magnitude of LTP was measured 60 min after tetanus and expressed as a percentage of baseline fEPSP peak amplitude.

Statistics. Datasets were compared by bifactorial (2 × 2) ANOVA or two-tailed Student *t* test where appropriate, using either raw or tied-ranked values. Threshold for significance was set at $P < 0.05$.

Additional methods and the associated references are provided in *SI Materials and Methods*.

ACKNOWLEDGMENTS. The authors thank Drs. M. Greenberg and D. Ginty for DNA constructs; Drs. Giuseppe Maulucci and Vito Vetrugno for critically reading the manuscript; and the laboratory members for experimental contributions and valuable suggestions. This study was funded by Grant EASD/Glaxo Smith Kline from the European Association for the Study of Diabetes and Grant IG8634/2009 from the Italian Association for Cancer Research (to G.P.), and by Catholic University intramural Grants Linea D.1 (to G.P.), D3.2 (to C.G.), and D3.2 (to T.G.). S.F. is the recipient of a Research Doctorate Fellowship from the Italian Ministry of University.

1. Fontana L, Partridge L, Longo VD (2010) Extending healthy life span—From yeast to humans. *Science* 328:321–326.
2. Maalouf M, Rho JM, Mattson MP (2009) The neuroprotective properties of calorie restriction, the ketogenic diet, and ketone bodies. *Brain Res Brain Res Rev* 59: 293–315.
3. Takeda S, et al. (2010) Diabetes-accelerated memory dysfunction via cerebrovascular inflammation and Abeta deposition in an Alzheimer mouse model with diabetes. *Proc Natl Acad Sci USA* 107:7036–7041.
4. de la Monte SM (2009) Insulin resistance and Alzheimer's disease. *BMB Rep* 42: 475–481.

5. Haigis MC, Guarente LP (2006) Mammalian sirtuins—Emerging roles in physiology, aging, and calorie restriction. *Genes Dev* 20:2913–2921.
6. Finkel T, Deng CX, Mostoslavsky R (2009) Recent progress in the biology and physiology of sirtuins. *Nature* 460:587–591.
7. Cohen DE, Supinski AM, Bonkowski MS, Donmez G, Guarente LP (2009) Neuronal SIRT1 regulates endocrine and behavioral responses to calorie restriction. *Genes Dev* 23:2812–2817.
8. Qin W, et al. (2006) Neuronal SIRT1 activation as a novel mechanism underlying the prevention of Alzheimer disease amyloid neuropathology by calorie restriction. *J Biol Chem* 281:21745–21754.
9. Donmez G, Wang D, Cohen DE, Guarente L (2010) SIRT1 suppresses beta-amyloid production by activating the alpha-secretase gene ADAM10. *Cell* 142:320–332.
10. Riccio A, Ahn S, Davenport CM, Blendy JA, Ginty DD (1999) Mediation by a CREB family transcription factor of NGF-dependent survival of sympathetic neurons. *Science* 286:2358–2361.
11. Finkbeiner S (2000) CREB couples neurotrophin signals to survival messages. *Neuron* 25:11–14.
12. Zuccato C, et al. (2001) Loss of huntingtin-mediated BDNF gene transcription in Huntington's disease. *Science* 293:493–498.
13. Cui L, et al. (2006) Transcriptional repression of PGC-1alpha by mutant huntingtin leads to mitochondrial dysfunction and neurodegeneration. *Cell* 127:59–69.
14. Caccamo A, Maldonado MA, Bokov AF, Majumder S, Oddo S (2010) CBP gene transfer increases BDNF levels and ameliorates learning and memory deficits in a mouse model of Alzheimer's disease. *Proc Natl Acad Sci USA* 107:22687–22692.
15. Altarejos JY, Montminy M (2011) CREB and the CRTC co-activators: Sensors for hormonal and metabolic signals. *Nat Rev Mol Cell Biol* 12:141–151.
16. Gao J, et al. (2010) A novel pathway regulates memory and plasticity via SIRT1 and miR-134. *Nature* 466:1105–1109.
17. Halagappa VK, et al. (2007) Intermittent fasting and caloric restriction ameliorate age-related behavioral deficits in the triple-transgenic mouse model of Alzheimer's disease. *Neurobiol Dis* 26:212–220.
18. Mantamadiotis T, et al. (2002) Disruption of CREB function in brain leads to neurodegeneration. *Nat Genet* 31:47–54.
19. Bevins RA, Besheer J (2006) Object recognition in rats and mice: A one-trial non-matching-to-sample learning task to study 'recognition memory'. *Nat Protoc* 1:1306–1311.
20. Bourtchuladze R, et al. (1994) Deficient long-term memory in mice with a targeted mutation of the cAMP-responsive element-binding protein. *Cell* 79:59–68.
21. Koizumi H, Hashimoto K, Iyo M (2006) Dietary restriction changes behaviours in brain-derived neurotrophic factor heterozygous mice: Role of serotonergic system. *Eur J Neurosci* 24:2335–2344.
22. Nelson RJ, et al. (1995) Behavioural abnormalities in male mice lacking neuronal nitric oxide synthase. *Nature* 378:383–386.
23. Zhang X, et al. (2005) Genome-wide analysis of cAMP-response element binding protein occupancy, phosphorylation, and target gene activation in human tissues. *Proc Natl Acad Sci USA* 102:4459–4464.
24. Hori N, Hirotsu I, Davis PJ, Carpenter DO (1992) Long-term potentiation is lost in aged rats but preserved by calorie restriction. *Neuroreport* 3:1085–1088.
25. Balschun D, et al. (2003) Does cAMP response element-binding protein have a pivotal role in hippocampal synaptic plasticity and hippocampus-dependent memory? *J Neurosci* 23:6304–6314.
26. Nisoli E, Clementi E, Moncada S, Carruba MO (2004) Mitochondrial biogenesis as a cellular signaling framework. *Biochem Pharmacol* 67:1–15.
27. Rodgers JT, et al. (2005) Nutrient control of glucose homeostasis through a complex of PGC-1alpha and SIRT1. *Nature* 434:113–118.
28. Vaquero A, et al. (2004) Human SirT1 interacts with histone H1 and promotes formation of facultative heterochromatin. *Mol Cell* 16:93–105.
29. Riccio A, et al. (2006) A nitric oxide signaling pathway controls CREB-mediated gene expression in neurons. *Mol Cell* 21:283–294.
30. Impey S, et al. (2004) Defining the CREB regulon: a genome-wide analysis of transcription factor regulatory regions. *Cell* 119:1041–1054.
31. Nemoto S, Fergusson MM, Finkel T (2004) Nutrient availability regulates SIRT1 through a forkhead-dependent pathway. *Science* 306:2105–2108.
32. Vaziri H, et al. (2001) hSIR2(SIRT1) functions as an NAD-dependent p53 deacetylase. *Cell* 107:149–159.
33. Brunet A, et al. (2004) Stress-dependent regulation of FOXO transcription factors by the SIRT1 deacetylase. *Science* 303:2011–2015.
34. Sauve AA, Schramm VL (2003) Sir2 regulation by nicotinamide results from switching between base exchange and deacetylation chemistry. *Biochemistry* 42:9249–9256.
35. Du K, Asahara H, Jhala US, Wagner BL, Montminy M (2000) Characterization of a CREB gain-of-function mutant with constitutive transcriptional activity in vivo. *Mol Cell Biol* 20:4320–4327.
36. Peunova N, Enikolopov G (1995) Nitric oxide triggers a switch to growth arrest during differentiation of neuronal cells. *Nature* 375:68–73.
37. Boily G, et al. (2008) SirT1 regulates energy metabolism and response to caloric restriction in mice. *PLoS One* 3:e1759.
38. Altarejos JY, et al. (2008) The Creb1 coactivator Crtc1 is required for energy balance and fertility. *Nat Med* 14:1112–1117.
39. Cohen HY, et al. (2004) Calorie restriction promotes mammalian cell survival by inducing the SIRT1 deacetylase. *Science* 305:390–392.
40. Nisoli E, et al. (2005) Calorie restriction promotes mitochondrial biogenesis by inducing the expression of eNOS. *Science* 310:314–317.
41. Bedogni B, et al. (2003) Redox regulation of cAMP-responsive element-binding protein and induction of manganous superoxide dismutase in nerve growth factor-dependent cell survival. *J Biol Chem* 278:16510–16519.
42. Dawson VL, Dawson TM (1998) Nitric oxide in neurodegeneration. *Prog Brain Res* 118: 215–229.
43. St-Pierre J, et al. (2006) Suppression of reactive oxygen species and neurodegeneration by the PGC-1 transcriptional coactivators. *Cell* 127:397–408.

Supporting Information

Fusco et al. 10.1073/pnas.1109237109

SI Materials and Methods

Mice. The mutant mouse strain harboring a conditional cAMP responsive-element binding (CREB)-1 null allele (Exon 10) flanked by LoxP recombination sites (CREBflox transgenic mice) and the transgenic strain expressing the Cre recombinase under the control of the CAMK2A promoter (CaMK2a-iCre BAC), both originally developed by Schütz and colleagues (1, 2), were obtained from the European Mouse Mutant Archive (EMMA ID:02151 and EMMA ID: EM01153, respectively), Monterotondo, Italy. Mice were bred and maintained in the animal facility of the Catholic University Medical School. Animals were housed in a 12-h light/12-h dark cycle at controlled temperature (25 °C ± 1 °C). Genotyping was performed by PCR of genomic DNA from ear punches, according to above referenced protocols. In experimental procedures, we compared mice homozygous for *floxed* CREB (CREB $^{loxP/loxP}$) and heterozygous for CamK-*Cre* [Brain CREB KO (BCKO) mice] with CREB $^{loxP/loxP}$ littermates not expressing the recombinase (control mice). All mice were in the C57BL/6 genetic background and were housed individually.

All experimental procedures were performed according to international standards of Animal Care and had been previously approved by the "Comitato Etico" (Ethical Committee) of Universita' Cattolica.

Frozen brains from Sirt1 KO mice and their littermates (3) were shipped from M.W.M.'s laboratory to Catholic University in dry ice, and were immediately put in liquid nitrogen upon arrival and stored until processing for protein and RNA extraction.

Animal Studies. ***Calorie restriction.*** For calorie restriction (CR) studies, the amount of food consumed by ad libitum (AL) mice was determined weekly, and CR mice were fed daily 80% of that value for the first week and 60% for the following 4 wk. Absolute food consumption AL was slightly (about 10%) higher in control than in BCKO mice, but the amount of chow per gram body weight comparable, because of the smaller size of the latter strain. CR in BCKO mice was calculated either on the AL feeding of mice of the same genotype, or on the AL consumption of control mice, with similar results. Body weight was monitored weekly.

Behavioral tests. All behavioral tests were conducted on male, 6 mo-old mice, during the dark cycle (the animals' active phase). Before each test, mice were acclimatized to the experimental room for at least 30 min. The animals were subjected to several basal tests of locomotion, exploration, and anxiety to exclude differences that could influence behavioral tests. The tests were performed from least to more stressful with a pause of at least 48 h between individual tests.

Novel object recognition task. During training sessions, two novel objects were placed into an open-field box 14 inches away from each other (symmetrically) and then the individual animal was allowed to explore for 10 min. An explorative behavior was scored when the head of animal was facing close (less than 1 inch away) to object or any part of the body except the tail was touching the object. The time spent to explore each object was recorded. The animals were returned to their home cages immediately after training. During the retention test, one of the familiar objects used during training was replaced by a novel object, and the animals were allowed to explore freely for 10 min. All objects were balanced in terms of physical complexity and were emotionally neutral. Moreover, the open-field and objects were thoroughly cleaned by 70% alcohol after each session to avoid possible odorant cues. A preference index, a ratio of the amount of time spent exploring any one of the two items (training session) or the novel object (retention session) over the total time spent exploring both objects, was used to measure recognition memory. Two-way ANOVA (genotype X feeding regimen) and post hoc Tukey test were used to determine genotype and diet effects on the behavioral responses.

Resident-intruder paradigm. This test was performed according to Nelson et al. (4) with minor changes. The resident mice were housed individually 4 wk before the experiments, and the intruder mice were housed in groups of four. Adult, male stimulus mice (i.e., intruders) were introduced into the home cage of either a BCKO or a control adult male mouse. Intruder mice were marked on the tail with an indelible marker for purposes of identification. The bedding in the home cages remained unchanged for 10 d before testing. The latency to first aggressive encounter and the total number of aggressive encounters (bite attacks) initiated by the resident male were recorded. Aggression tests lasted 10 min and were conducted each day for 3 consecutive days at the same hour (normally 1500–1700 hours). Aggressive behaviors scored included chasing, biting, and offensive attacks. A novel pairing of animals was made for each consecutive test and intruder males were not used more than once per day. Raw or tied-ranked values were analyzed by two-way ANOVA test (genotype per feeding regimen), followed by Tukey post hoc test.

Long-term potentiation. Coronal hippocampal slices (400-μm thick) were prepared according to standard procedures (5) from three mice per experimental group. Slices were cut with a vibratome (VT1000S; Leica Microsystems) and incubated in the cutting solution [124 mM NaCl, 3.2 mM KCl, 1 mM NaH_2PO_4, 26 mM $NaHCO_3$, 2 mM $MgCl_2$, 1 mM $CaCl_2$, 10 mM glucose, 2 mM Na-pyruvate, and 0.6 mM ascorbic acid (pH 7.4, 95% O_2/5% CO_2)] at 30–32 °C for at least 60 min, and then stored in the same solution at room temperature until use. For electrophysiological recordings, slices were continuously perfused with artificial cerebrospinal fluid (aCSF) [124 mM NaCl, 3.2 mM KCl, 1 mM NaH_2PO_4, 1 mM $MgCl_2$, 2 mM $CaCl_2$, 26 mM $NaHCO_3$, and 10 mM glucose (pH 7.4, 95% O_2/5% CO_2)] in a submerged recording chamber. Flow rate was kept at 1.5 mL/min with a peristaltic pump (Minipuls 3; Gilson), and bath temperature was maintained at 30–32 °C with an in-line solution heater and temperature controller (TC-344B; Warner Instruments).

Field excitatory postsynaptic potentials (fEPSP) evoked by Schaffer collateral stimulation were recorded from the CA1 subfield of the hippocampus. For this purpose, a glass capillary microelectrode filled with aCSF (tip resistance 2–5 MΩ) and a stimulating bipolar tungsten electrode were positioned into the stratum radiatum of CA1. Hippocampal subfields and electrode positions were identified with the aid of 4× and 40× water immersion objectives on an upright microscope equipped with differential interface contrast optics under infrared illumination (BX5IWI; Olympus) and video observation (C3077-71 CCD camera; Hamamatsu Photonics). Data acquisition and stimulation protocols were performed with the Digidata 1440 Series interface and pClamp 10 software (Molecular Devices). Data were filtered at 1 kHz, digitized at 10 kHz, and analyzed both online and offline. Input/output curves were built by plotting the amplitudes of fEPSPs versus stimulus intensity. The stimulation intensity that elicited one-third of the maximal response was used for delivering test pulses and tetanus.

After 20–30 min of stable baseline responses to test stimulations delivered once every 20 s, long-term potentiation (LTP) was induced with a standard stimulation paradigm referred to as "teta-

nus" (four trains, 500 ms each, 100 Hz within the train, repeated every 20 s).

Responses to test pulses were then recorded every 20 s for 60 min to measure LTP. The magnitude of LTP was measured 60 min after tetanus and expressed as a percentage of baseline fEPSP peak amplitude. The mean values observed during the last 10 min of pretetanus recordings were considered to represent 100%. Reported fEPSP amplitudes at 60 min are averages from recordings obtained during the last 10 min of posttetanus recordings.

Immunohistochemistry. Anesthetized mice were transcardially perfused with Ringer's solution followed by 4% paraformaldehyde–lysine–periodate fixative solution. The brain was removed from the skull, postfixed overnight at 4 °C, and then transferred to a solution of 30% sucrose in PBS for 2 d. Sagittal or coronal brain sections (35-μm thick) were then cut with a vibratome (VT1000S; Leica Microsystems), and floated in ice-cold PBS. Sections were collected and stored until use in cryoprotectant at −20 °C.

For assessment of CREB expression, sections were blocked for 1 h at room temperature in 1% BSA solution containing 10% normal goat serum and 0.5% Triton X-100 (Sigma). The sections were then incubated for 48 h at 4 °C with the primary antibodies (rabbit monoclonal anti-CREB, 1:400; Cell Signaling Technology), washed several times in PBS, and incubated with secondary antibody (Alexa-488 donkey anti-rabbit IgG, 1:300; Invitrogen). Finally, brain slices were incubated with DAPI (0.5 μg/mL; Invitrogen) to stain cell nuclei, and the sections were mounted on glass slides and cover-slipped with ProLong Gold antifade reagent (Invitrogen).

Images were obtained with a fluorescence microscope (BX5I; Olympus) equipped with a professional digital compact camera (*CAMEDIA,* C5050 ZOOM; Olympus).

Chromatin Immunoprecipitation. ChIP assays were performed largely as described (6, 7). For all cell types, ~1 to 3×10^6 cells were used per ChIP. Briefly, at the end of stimulations formaldehyde (1%) was added directly to the medium for 10 min; afterward, medium was removed from treated cells and replaced with PBS containing protease inhibitors. Cells were rinsed twice and harvested in PBS, collected by centrifugation, and pellets were resuspended in 200 μL lysis buffer containing SDS (1%), Tris-HCl (pH 8.1, 50 mM), and EDTA (10 mM). Samples were sonicated on ice with eight 10-s pulses with a 10-s interpulse interval.

Cell debris was removed by centrifugation, and supernatants were precleared by incubation with protein-G Sepharose 4B beads (Sigma-Aldrich) for 1 h at 4 °C. Beads were collected by centrifugation and supernatants were subjected to immunoprecipitation. A fraction of the supernatant was used for total input control. The volume of each tube was adjusted to 2 mL with dilution buffer (0,01% SDS, 1% Triton X-100, 1,2 mM EDTA, 16,7 mM Tris HCl pH 8.1, 167 mM NaCl) and split in equal volumes for each immunoprecipitation; 2–4 μg of specific antibody or rabbit IgG was added overnight at 4 °C. Immune complexes were collected by incubation with protein-G Sepharose 4B beads for 2 h at 4 °C. Beads were collected and subjected to a series of seven sequential washes. Two washes each were performed in lysis buffer and then in washing buffer containing SDS (0.1%), Triton X-100 (0.5%), EDTA (pH 8.0, 2 mM), Tris-HCl (pH 8.1, 20 mM), and NaCl (150 mM). One wash was performed in lithium buffer containing LiCl (0.25 M), Nonidet P-40 (1%), deoxycholate (1%), EDTA (pH 8.0, 1 mM), and Tris-HCl (pH 8.1, 10 mM). Two final washes were performed in 1× TE (pH 8.1). Immune complexes were eluted from beads by vortexing in elution buffer containing SDS (1%) and NaHCO3 (pH 8.0, 0.1 M). NaCl was added (final concentration 0.33 M), and cross-linking was reversed by incubation overnight at 65 °C. DNA fragments were purified by using the Nucleospin extract II PCR purification kit (Macherey-Nagel). For PCR, specific sets of primers were designed that flank CRE regions within the upstream regulatory regions of the indicated genes. PCR conditions and cycle numbers were determined empirically for the different templates and primer pairs. Primers amplified fragments ranging in size from 200 to 400 bp. Primer sequences and PCR conditions are available on request.

Statistics. Datasets were compared by bifactorial (2 × 2) ANOVA or two-tailed Student *t* test where appropriate, using either raw or tied-ranked values. Threshold for significance was set at $P < 0.05$ unless indicated.

Reagents and Antibodies. Most of the Chemicals were obtained from Sigma-Aldrich. Forskolin (Fsk) was from BIOMOL/Enzo Life Sciences Inc.; NGF was a kind gift of Antonella Riccio (Medical Research Council, London, United Kingdom).

Polyclonal rabbit antibodies against CREB1 (cat#AB3006), p-Ser133-CREB (cat#06–519), anti-Sir2.1 (cat#07–131) and Histone H4 (cat#07–108), and the anti–Acetyl-Lysine mouse monoclonal antibody (cat.#05–515) were from Upstate Biotechnology/Millipore; anti-actin (goat polyclonal, cat #sc-1615 and sc-1616), anti Sirt-1 rabbit polyclonal (sc15404) and myc-tag monoclonal antibody (clone 9E10, sc-40) were from Santa Cruz Biotechnology; anti–Ac-H4K16 (H9164) and anti–Ac-H3K9 (H9286) rabbit anti-sera were from Sigma. Anti-Histone H3 mouse monoclonal antibody was from Abcam (ab10799).

The Ultrasensitive (Mouse) Insulin Elisa Kit (cat. # 80-INSMSU-E01) was purchased from Alpco Immunoassays.

The transfection reagent Lipofectamine 2000 was obtained from Invitrogen.

Cell Lines, Viral Vectors, and Plasmids. PC12 rat pheochromocytoma cells were obtained from ATCC. Cells were maintained in RPMI medium 1640 containing 10% (vol/vol) FCS and 5% (vol/vol) horse serum.

A ~450-bp genomic region surrounding two half-CREs located 1,998 and 2,012 bp downstream of the transcription start site in the mouse *Sirt1* gene was amplified by PCR with primers harboring KpnI (forward) and XhoI (reverse) restriction sites, and cloned in the MCS of the pGL3 luciferase reporter vector (Promega). The construct was verified by DNA sequencing.

Replication-deficient (ΔE1/ΔE3) human adenoviral vector type 5-expressing Cre recombinase under the transcriptional control of the cytomegalovirus promoter was constructed by homologous recombination in *Escherichia coli* using the Ad-Easy System (8). Full-length cDNA coding for the P1 bacteriophage Cre recombinase was derived from the pBS185 plasmid (9) and inserted into the pShuttle-CMV plasmid. Propagation in human embryonic kidney 293T cells and purification of the adenoviral vectors by cesium chloride gradient ultracentrifugation were performed as described previously (10). Viral titers were determined by serial dilution on 293 cells and were expressed as plaque-forming units per milliliter (PFU/mL). Adenoviral stocks were tested for the absence of replication-competent adenoviruses by a A549 cells assay (10).

A third-generation self-inactivating lentiviral vector (LV) expressing the human Sirt-1 was generated by cloning the full-length cDNA for Sirt-1 derived from the pYESir2-Puro plasmid (11) in replacement to the E-GFP cDNA into the pCCLsin. cPPT.hPGK.E-GFP.Wpre (phosphoglycerate kinase promoter–enhanced jellyfish GFP) construct, obtained from E. Vigna (Istituto Di Ricovero e Cura a Carattere Scientifico, Candiolo, Italy). Recombinant vesicular stomatitis virus-pseudotyped LVs were obtained as previously described (12).

The pYESir2-Puro plasmid encoding the human Sirt-1 cDNA in the pBabe-Y-Puro vector backbone was kindly provided by Michael Greenberg (Harvard Medical School, Boston, MA). Human CREB1 and CREB1-ΔLZ cDNAs inserted (EcoRI-

BglII) in the pCMV-Myc vector (Clontech Laboratories) were a gift of David Ginty (The Johns Hopkins University, Baltimore, MD). The pFC-PKA construct encoding the catalytic subunit of the c-AMP dependent protein kinase under the transcriptional control of the CMV promoter was obtained from STRATAGENE/Agilent Technologies.

Transfection of plasmids and siRNA duplexes into undifferentiated PC12 rat pheochromocytoma cells was performed using lipofectamine 2000, according to the manufacturer's recommendations.

Studies in Vitro. ***Culture and infection of primary neurons.*** Primary cultures of cortical and hippocampal neurons were obtained from E18 lox/lox mice embryos according to standard procedures. Briefly, for cortical neurons, cortices were dissected and incubated for 10 min at 37 °C in PBS containing 0.025% trypsin/0.01% EDTA (Biochrom AG). The tissue was then mechanically dissociated at room temperature (23–25 °C) using a fire-polished Pasteur pipette and the cell suspension was harvested and centrifuged at 100 × *g* for 8 min. The pellet was suspended in 88.8% (vol/vol) minimum essential medium (Biochrom), 5% FBS, 5% (vol/vol) horse serum, 1% glutamine (2 mM), 0.2% gentamicin (0.1 mg/mL) and glucose (25 mM). Cells were seeded on 6-, 12-, and 24-well plates precoated with poly-L-lysine (0.1 mg/mL; Sigma) at a density of 1×10^6, 5×10^5, 2.5×10^5 cells per well, respectively. At 24 h after plating, the culture medium was replaced with a medium containing 97.3% (vol/vol) neurobasal medium (Invitrogen), 2% (vol/vol) B-27 (Invitrogen), 0.5% glutamine (2 mM), and 0.2% gentamicin (0.1 mg/mL). After 72 h, the culture medium was replaced with a similar medium lacking glutamine and supplemented with 2 μM cytosine β-D-arabinofuranoside to inhibit glial cell proliferation. For hippocampal primary cultures, the hippocampi were dissected in ice cold HBSS and incubated with papain solution for 1 h at 37 °C with gentle shaking. Tissues were mechanically dissociated by gentle trituration and were plated at the same density described for cortical neurons.

The cultures were maintained at 37 °C in a humidified atmosphere of 5% CO_2 until experimental procedures.

For primary culture transduction neurons [days in vitro (DIV) 5] were infected with 10 PFU/cell of each adenovirus or lentivirus vector: half of the medium was replaced with fresh medium after 6 h and again after 48 h. After 6 d from infection the neurons (DIV11) were stimulated and harvested for mRNA and protein isolation or quantification of cell survival.

Analysis of cell survival. For MTT assay, neurons were seeded in 24-well plates (2.5×10^5/mL) and infected at DIV5 to delete CREB and/or overexpress SIRT1. After 6 d (DIV11) H_2O_2 (100 μM) was added to the medium and on the day of the assay (DIV12, after 24 h from the treatment) solutions were removed and replaced with fresh culture medium. MTT solution (1:10 dilution of the 5-mg/mL stock) was added and incubated at 37 °C for 3 h. The medium and MTT solution were then removed, and the converted dye was solubilized with 500 μL of acidic isopropanol (0.04 M HCl in absolute isopropanol). Absorbance was read at 570 nm. Data are the average of three wells, and the experiment was repeated three times with similar results.

PC12 differentiation. For differentiation into sympathetic neurons, PC12 cells were seeded at 2 to 5×10^4 cells per well in collagen-coated 12-well plates 16 h before transfection with 100 nmols of siCtrl or siSirt-1 RNA duplexes. After 3 d (day 0), medium was replaced and NGF was added at 50 ng/mL immediately and again after 36 h (day+1.5). At day +3 early differentiated cells (i.e., cells with processes longer than one cell body) were counted under the phase-contrast microscope. Percentage of differentiated cells was determined in 10 randomly chosen fields from different wells. Datasets were compared by two-tailed Student's *t*-test.

Analysis of gene expression. For mRNA isolation, retrotranscription and amplification, total RNA was extracted using QIAzol Lysis reagent (Qiagen) according to the the manufacturer's instructions. One to two micrograms of total RNA was reverse-transcribed by extension of oligodT (Fermentas) primers using M-MLV (USB) reverse transcriptase. PCR of the cDNA was performed using Taq Polymerase (Fischer) with the following pairs of primers:

PGC-1 (rat/mouse) Forward: GGAGACGTGACCACTGACA
PGC-1 (rat/mouse) Reverse: TCAATAGTCTTGTTCTCAAATG
SIRT1 (rat/mouse/human) Forward: TTTCATTCCTGTGAAAGTGATG
SIRT1 (rat/mouse/human) Reverse: CAAACTTGAAGAATGGTCTTG
nNOS Forward (rat/mouse): CTGTGACAACTCTCGATACAACATC
nNOS Reverse (rat/mouse): GAGTCTATAGTTGAGCATCTCCTGG
actin Forward (rat/mouse): GTCACCCACACTGTGCCCATCT
actin Reverse (rat/mouse): ACCGAGTACTTGCGCTCAGGA
PEPCK Forward (rat/mouse): GCAGCATGGGGTGTTTGTAGG
PEPCK Reverse (rat/mouse): AACAGCTCCTCCACGTTGACG
CREB Forward (rat/mouse/human): AGCCATCAGTTATTCAGTCTC
CREB Reverse (rat/mouse/human): AGTGCTTTTAGCTCCTCAATC

Sequences of primer sets used for peroxisome proliferator-activated receptor-γ coactivator-1α (PGC-1α) targets displayed in Fig. S2 can be provided by the authors upon request.

The PCR program used was: 2 min at 94 °C, followed by 33 cycles (30 s at 94 °C, 30 s at 56–60 °C, 40 s at 72 °C), followed by 7 min extension at 72 °C. A PCR was also performed on total RNA that had not been reverse-transcribed to control for the absence of genomic DNA in the RNA preparation. The products of the PCR reactions were resolved on a 1% agarose gel.

Luciferase Reporter Assay. Cells (PC12) were cotransfected (ratio 50:50:1) with the Sirt1-luc reporter, the PKA expression vector (or an empty control), and a plasmid encoding the *Renilla* luciferase under the control of the CMV promoter as an internal transfection control. Forty-eight hours later and after the appropriate stimulations, cells were lysed directly in the culture plate with Passive Lysis Buffer, and Firefly/*Renilla* luciferase activity measured with by a Dual Luciferase Assay Kit (Promega) and a portable luminometer (Junior LG 9509; Berthold Technologies), according to the manufacturer's instructions.

Protein Studies. For protein expression/phosphorylation studies cells were lysed in ice-cold lysis buffer (NaCl 150 mM, Tris-Hcl 50 mM pH 8; 2 mM EDTA) containing 1% vol/vol Triton X-100, 0.1% vol/vol SDS, 1:1,000 Protease Inhibitor mixture (Sigma), 1 mM Sodium Orthovanadate, 1 mM NaF, and 2 mM β-glycerophosphate. After 15 min on ice with occasional vortexing, cells were spun down at 22,000 × *g*, 4 °C to remove debris and unlysed cells, and supernatant quantified for protein content (DC Protein Assay; Bio-Rad), resuspended in 6× Laemmli buffer, boiled, and subdued SDS-PAGE.

For immunoprecipitation (or coimmunoprecipitation) studies, cells/tissues were lysed in low detergent (0.2% Nonidet P-40) buffer and lysates were precleared with empty protein G-sepharose 4B beads (Sigma) before being challenged with specific or control antisera and fresh protein G matrix. After 3 h incubation at 4 °C with continuous agitation, protein-G bound immunocomplexes were collected by centrifugation (22,000 × *g*,

30 s) and washed six times in immunoprecipitation buffer. Beads were finally resuspended in 40 μL of 1× Laemmli buffer and boiled. Eluted proteins were subjected to SDS-PAGE and immunoblotting.

1. Casanova E, et al. (2001) A CamKIIalpha iCre BAC allows brain-specific gene inactivation. *Genesis* 31:37–42.
2. Mantamadiotis T, et al. (2002) Disruption of CREB function in brain leads to neurodegeneration. *Nat Genet* 31:47–54.
3. Boily G, et al. (2008) SirT1 regulates energy metabolism and response to caloric restriction in mice. *PLoS One* 3:e1759.
4. Nelson RJ, et al. (1995) Behavioural abnormalities in male mice lacking neuronal nitric oxide synthase. *Nature* 378:383–386.
5. Cuccurazzu B, et al. (2010) Exposure to extremely low-frequency (50 Hz) electromagnetic fields enhances adult hippocampal neurogenesis in C57BL/6 mice. *Exp Neurol* 226:173–182.
6. Weinmann AS, Farnham PJ (2002) Identification of unknown target genes of human transcription factors using chromatin immunoprecipitation. *Methods* 26:37–47.
7. Wells J, Farnham PJ (2002) Characterizing transcription factor binding sites using formaldehyde crosslinking and immunoprecipitation. *Methods* 26:48–56.
8. He TC, et al. (1998) A simplified system for generating recombinant adenoviruses. *Proc Natl Acad Sci USA* 95:2509–2514.
9. Sauer B, Henderson N (1990) Targeted insertion of exogenous DNA into the eukaryotic genome by the Cre recombinase. *New Biol* 2:441–449.
10. Ross PJ, Parks RJ (2009) Construction and characterization of adenovirus vectors. *Cold Spring Harb Protoc*, 10.1101/pdb.prot5011.
11. Vaziri H, et al. (2001) hSIR2(SIRT1) functions as an NAD-dependent p53 deacetylase. *Cell* 107:149–159.
12. Follenzi A, Naldini L (2002) HIV-based vectors. Preparation and use. *Methods Mol Med* 69:259–274.

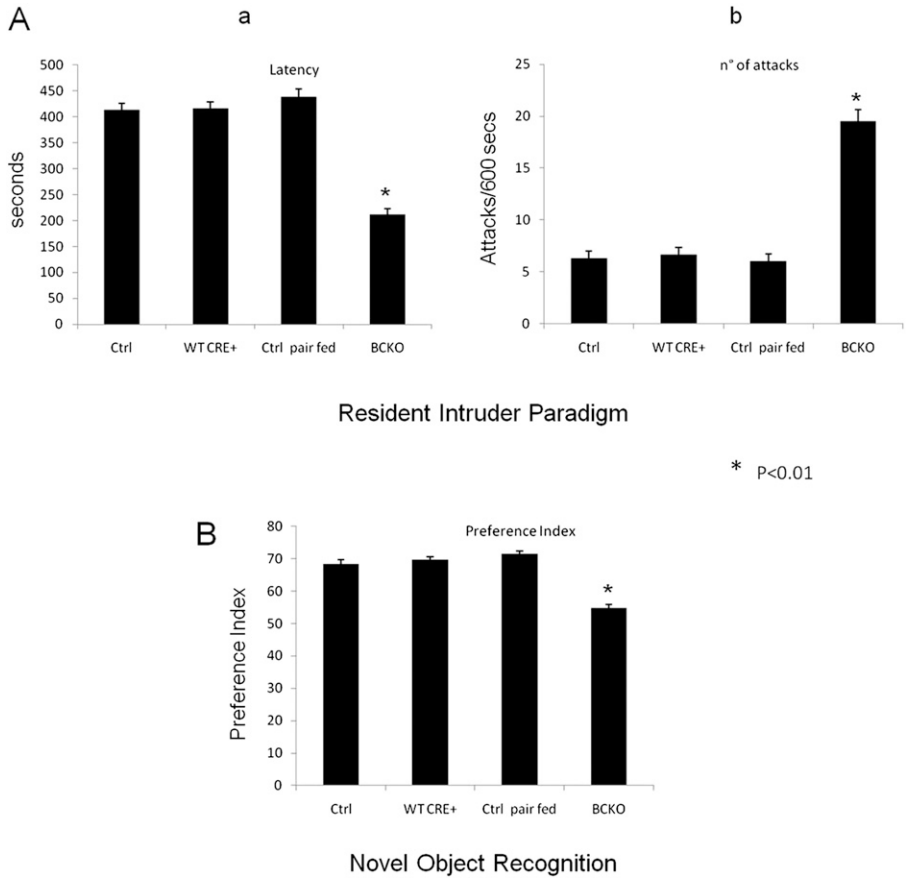

Fig. S1. (*A* and *B*) Behavioral differences between control (Ctrl) and BCKO mice are independent of Cre recombinase expression and AL food intake. The following groups of mice ($n = 6$) were compared: Ctrl and BCKO, as in Fig. 1; Cre+, CREB WT mice expressing the Cre transgene; Ctrl pair fed, Ctrl mice (CREB loxP/loxP Cre-) fed the same amount of chow as BCKO AL. The only significant difference is indicated by the asterisk ($P < 0.01$ by One-way ANOVA).

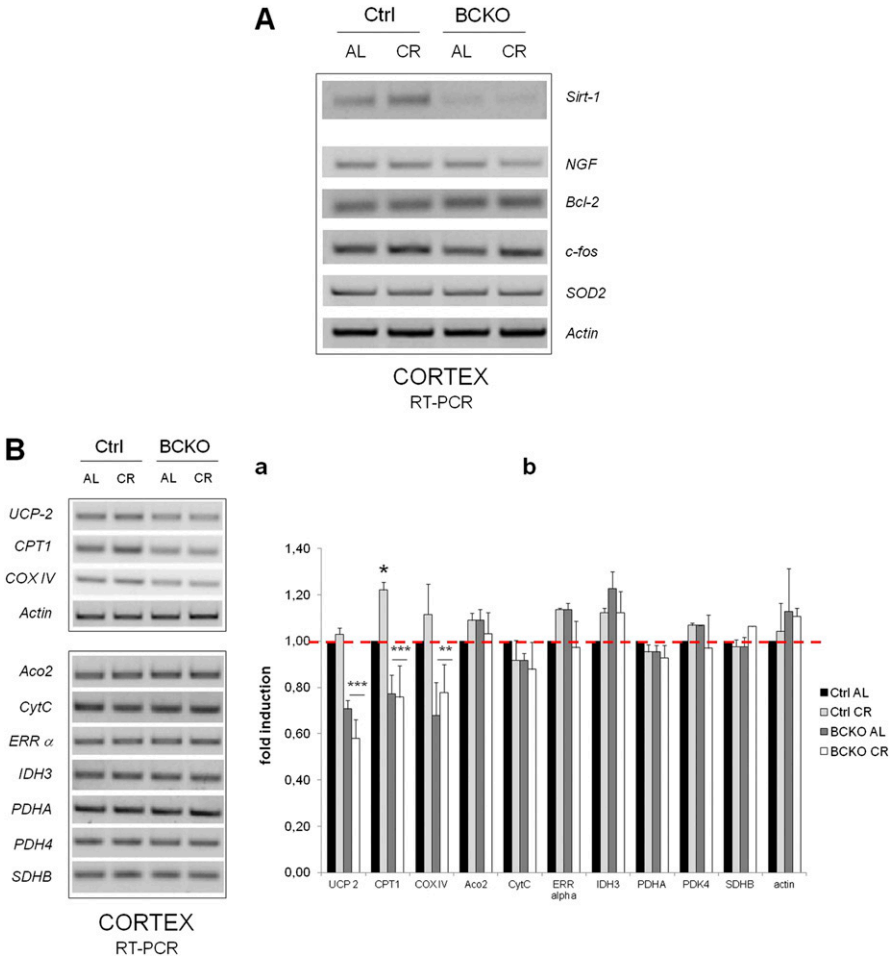

Fig. S2. (*A*) The cortical expression of some canonical CREB target genes is unaffected by CR and CREB deletion. RT-PCR analysis of brain cortex total RNA from AL and CR individual mice of the indicated genotypes. A number of putative CREB target mRNAs were retro-transcribed and amplified with specific primer sets. No relevant changes as a function of mouse genotype or feeding regimen were observed for *NGF*, *Bcl-2*, *c-fos*, and *SOD2*. Actin mRNA was amplified as input control. The expression pattern of *Sirt-1* in the same samples is also reported for comparison; note that the Sirt-1 gel displayed here is different from the one shown in Fig. 2*Ca*. (*B*) Effect of CREB deletion and CR on the expression of a number genes putatively regulated by PGC-1α in mouse cortex. (*a*) Expression of the indicated mRNAs was assessed by semiquantitative RT-PCR in individual mice representative of each genotype and feeding regimen. Transcripts that displayed the most evident changes by BCKO and/or CR were grouped in the *Upper* panel together with actin as input RNA control. The following genes were analyzed: Aconitase 2 (Aco2), Cytochrome oxidase subunit IV (COX IV), Carnitine Palmitoyl Transferase 1 (CPT 1), Cytochrome C (CytC), Isocitrate Dehydrogenase (IDH) 3, Pyruvate Dehydrogenase subunit A (PDHA), Pyruvate Dehydrogenase Kinase (PDK) 4, Succinate Dehydrogenase subunit B (SDHB), Estrogen recetor (ERR α), Uncoupling Protein (UCP) 2, actin. Genes were selected based on ref. 1. (*b*) Histogram displaying fold-changes of the mRNAs from *a* compared with the Ctrl AL group; values are mean± SD of $n = 3$ mice. Significant differences by two-way ANOVA are indicated. *$P < 0.05$ Ctrl AL vs. Ctrl CR; ** and ***: $P < 0.001$ and $P < 0.0001$ BCKO vs. Ctrl ("row effect").

1. Schreiber SN, et al. (2004) The estrogen-related receptor alpha (ERRalpha) functions in PPARgamma coactivator 1alpha (PGC-1alpha)-induced mitochondrial biogenesis. *Proc Natl Acad Sci USA* 101:6472–6477.

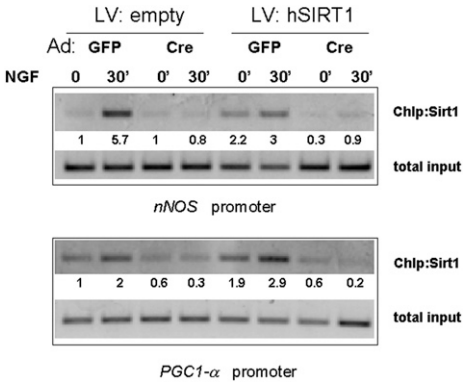

Fig. S3. Overexpression of hSirt-1 in CREB-deficient neurons does not rescue sirtuin interaction with CREB target promoters. CREBloxP/loxP hippocampal cells were infected with the indicated combinations of adenoviral (Ad-GFP or Ad-Cre) and lentiviral (LV-empty or LV-hSirt1) vectors to achieve deletion of CREB, overexpression of Sirt-1 or the two events in combination. Sirt1 binding to the promoter region of neuronal NO Synthase (nNOS) and peroxisome proliferator-activated receptor-γ coactivator 1α (PGC-1α) was determined by ChIP in resting and NGF-stimulated neurons. Note that basal and NGF-induced interaction of Sirt1 with both promoters is drastically reduced CREB-deleted cells irrespective of Sirt1 overexpression. Numbers are band densitometric values relative to lane 1. Amplification of total chromatin is displayed as input control.

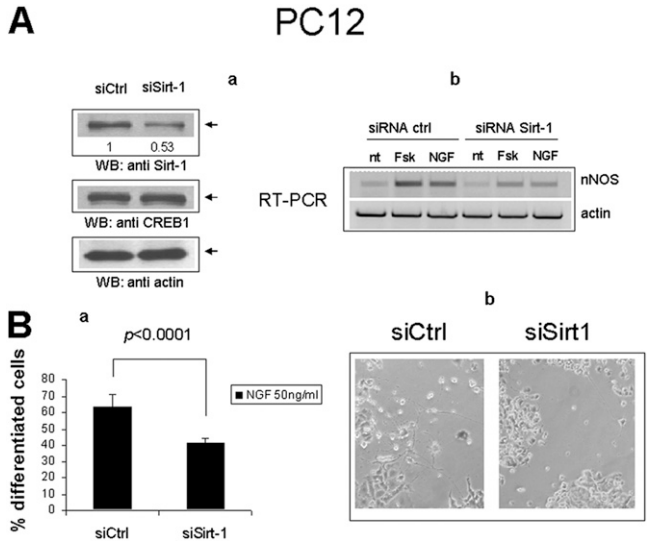

Fig. S4. Sirt1 knock-down inhibits induction of nNOS and differentiation of PC12 cells by NGF. (*Aa*) Western blot analysis of protein extracts from cells treated with Sirt-1 specific (siSirt-1) or irrelevant (siCtrl) RNA duplexes. Bands corresponding to Sirt-1, CREB, and actin are indicated by arrows. Numbers indicate relative optical density of the Sirt-1 bands. (*b*) Semiquantitative RT-PCR analysis of nNOS mRNA in naive PC12 cells 3 d after treatment with irrelevant or Sirt-1 specific siRNA duplexes. CREB-dependent stimuli (Fsk, 10 μM; NGF 50 ng/mL) are indicated. Actin amplification confirms equal input RNA throughout the lanes. (*Ba*) Differentiated cells were counted 72 h after exposure to NGF. Values are the mean percentage of differentiated cells over ten randomly chosen microscopic fields (about 1,000 total cells) ± SD. Datasets were compared by two-tailed Student *t* test. (*b*) Phase-contrast microphotographs of two representative microscopic fields. (Magnification: 100×.) Cells with processes longer than the cell body were scored as differentiated (details in *Materials and Methods*).

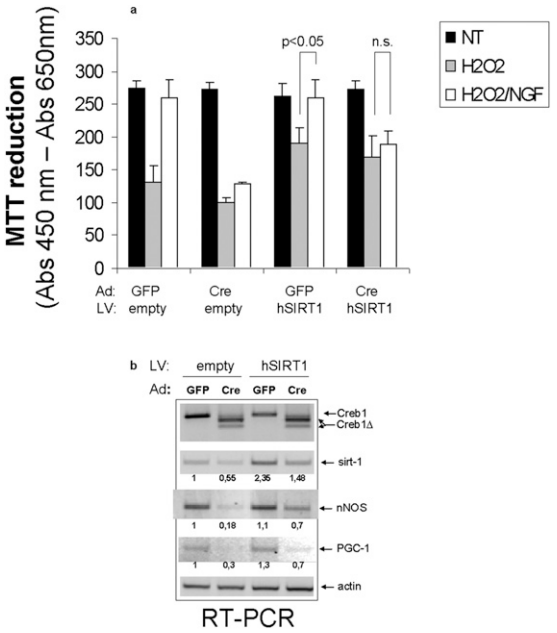

Fig. S5. Overexpression of human Sirt-1 does not rescue cell protection by NGF in CREB-deficient neurons. (*A*) Hippocampal neurons were infected with the same lenti/adenoviral mixtures as in Fig. S3; 3 d after infections cells were challenged with 100 mM hydrogen Peroxide (H_2O_2) in the presence or absence of NGF (50 ng/mL), or left untreated (NT). After 24 h of incubation, viability was determined by the MTT reduction assay. Figure representative of two independent experiments each performed in triplicate. Two relevant comparisons by Student's *t*-test are indicated. (*B*) Semiquantitative RT-PCR analysis of total RNA from NGF-stimulated hippocampal neurons infected as in *A*. Bands corresponding to *CREB1, Sirt-1, nNOS,* and *PGC-1α* are indicated by arrows. Primers for *Sirt-1* match perfectly both human and murine cDNA. Numbers are band intensities relative to the first lane. Picture representative of two independent experiments.

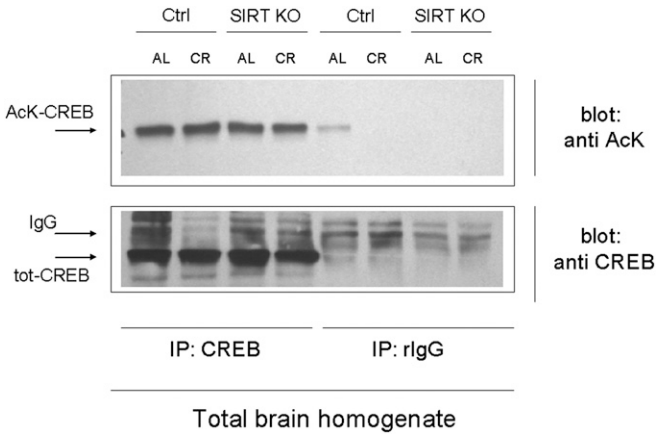

Fig. S6. Sirt-1 deletion and CR do not affect CREB acetylation in whole mouse brains. Brain homogenates from Ctrl and Sirt1 KO mice fed AL or under CR regimen were immunoprecipitated with an anti-CREB antiserum, and immunocomplexes immunostained with a mouse anti Acetyl-Lysine antibody (*Upper*) or with the same rabbit antiserum used for immunoprecipitation. Mock (rabbit IgG) immunoprecipitations were also performed as negative controls. Relevant bands, and an aspecific IgG band recognized by the secondary reagent, are indicated by arrows; samples are from one mouse for each strain per treatment. (*Upper*) A weak aspecific signal in lane 5 is probably because of spill-over from lane 4.

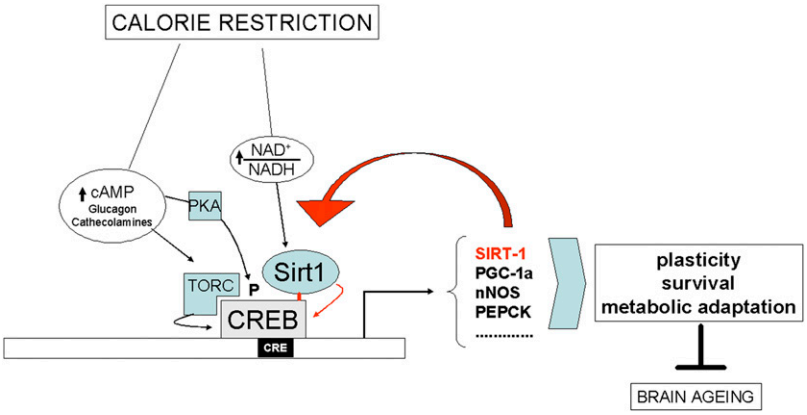

Fig. S7. Role of CREB and Sirt-1 in brain response to calorie restriction. Model depicting multiple mechanisms whereby reduced nutrient intake activates CREB; these include (*i*) metabolic activation of Sirt-1 molecules recruited to CREB-dependent promoters, (*ii*) hormone/cAMP-induced phoshorylation of CREB, and (*iii*) induction of the CREB coactivator TORC (1). CREB-induced genes enhance neuronal plasticity, survival and metabolic adaptation, thus delaying brain aging; up-regulation of Sirt-1 bolsters the protective response, establishing a feed-forward loop. Interactions demonstrated or suggested by the present work are highlighted in red.

1. Altarejos JY, Montminy M (2011) CREB and the CRTC co-activators: Sensors for hormonal and metabolic signals. *Nat Rev Mol Cell Biol* 12:141–151.